PCCP

Theoretical Study on the Microscopic Mechanism of Lignin Solubilization in Keggin-type Polyoxometalate Ionic Liquids

Journal:	*Physical Chemistry Chemical Physics*
Manuscript ID	CP-ART-09-2019-005339.R1
Article Type:	Paper
Date Submitted by the Author:	07-Dec-2019
Complete List of Authors:	Ju, Zhaoyang; China Agricultural University, College of Engineering Xiao, Weihua; China Agricultural University, College of Engineering Yao, Xiaoqian; Chinese Academy of Science, Institute of Process Engineering, Tan, Xin; Chinese Academy of Science, Institute of Process Engineering Simmons, Blake; E O Lawrence Berkeley National Laboratory, Biological Systems and Engineering Sale, Kenneth; Joint BioEnergy Institute, Deconstruction; Sandia National Laboratories, Biomass Science and Conversion Technology Sun, Ning; Lawrence Berkeley National Laboratory, Physical Biosciences

Theoretical Study on the Microscopic Mechanism of Lignin Solubilization in Keggin-type Polyoxometalate Ionic Liquids

Zhaoyang Ju[a,b,c], Weihua Xiao[a], Xiaoqian Yao[f], Xin Tan[f], Blake A. Simmons,[c,d], Kenneth L. Sale[c, e], Ning Sun[b*]*

[a]*Engineering Laboratory for AgroBiomass Recycling & Valorizing, College of Engineering, China Agricultural University, Beijing, China*

[b]*Advanced Biofuel and Bioproducts Process Development Unit (ABPDU), Lawrence Berkeley National Laboratory, Berkeley, CA, USA*

[c]*Joint BioEnergy Institute, Lawrence Berkeley National Laboratory, Berkeley, CA, USA*

[d]*Lawrence Berkeley National Laboratory, Berkeley, CA, USA*

[e]*Sandia National Laboratories, Livermore, CA, USA*

[f]*CAS Key Laboratory of Green Process and Engineering, Beijing Key Laboratory of Ionic Liquids Clean Process, State Key Laboratory of Multiphase Complex Systems, Institute of Process Engineering, Chinese Academy of Sciences, Beijing, China*

Abstract

Keggin-type polyoxometalate derived ionic liquids (POM-ILs) have recently been presented as effective solvent systems for biomass delignification. To investigate the mechanism of lignin dissolution in POM-ILs, the system involving POM-IL ($[C4C1Im]_3[PW_{12}O_{40}]$) and guaiacyl glycerol-β-guaiacyl ether (GGE), which contains a β-O-4 bond (the most dominant bond moiety in lignin), was studied using quantum mechanical calculations and molecular dynamics simulations. These studies show that more stable POM-IL structures are formed when $[C4C1Im]^+$ is anchored in the connecting four terminal oxygen region of the $[PW_{12}O_{40}]^{3-}$ surface. The cations in POM-ILs appears to stabilize the geometry by offering strong and positively charged sites, and the POM anion is a good H-bond acceptor. Calculations of POM-IL interacting with GGE show the POM anion interacts strongly with GGE through many H-bonds and π-π interactions which

are the main interactions between the POM-IL anion and GGE and are strong enough to force GGE into highly bent conformations. These simulations provide fundamental models of the dissolution mechanism of lignin by POM-IL, which is promoted by strong interactions of the POM-IL anion with lignin.

Keyword

Lignin, Polyoxometalate, Ionic liquids, Dissolution, Mechanism, Theoretical Simulations.

1. Introduction

Lignin is a complex, recalcitrant biopolymer composed of three types of phenylpropanoid monomers, guaiacylpropane (G), *p*-hydroxyphenylpropane (H) and syringylpropane (S), linked together via aryl ether (β-O-4, α-O-4), phenylcoumaran (β-5), resinol (β-β), biphenyl ether (4-O-5) and dibenzodioxocin (5-5) bonds[1], with β-O-4 bonds representing more than half of the linkage structures present in most of the common forms of lignin.[2, 3] It is the most abundant source of renewable aromatics on the planet and upgrading it to value added fuels and chemicals is key to the economic viability of lignocellulosic biofuels.[4] As a first step to valorization, lignin must be depolymerized to fragments amenable to upgrading; however, efficient depolymerization of the complex recalcitrant polymer continues to present significant challenges.[5, 6]

To develop successful and commercially viable routes to depolymerizing lignin into targeted intermediates, homogeneous and heterogeneous catalytic processes for both oxidative and reductive lignin depolymerization have been reported.[2, 7, 8] Among these approaches, Keggin-type Polyoxometalates (POMs) have shown great promise. POMs are transition metal oxide anionic clusters composed of d^0 metal cations (W^{VI}, Mo^{VI}, and V^{V}) in different combinations, with or without a guest atom located in the center of the metal-oxygen cage[9]. Since the mid-1990s, considerable attention has been paid to POMs combined with oxygen for pulp bleaching. It has been shown that POMs together with O_2 constitute a promising system for pulp delignification through lignin oxidation. POMs can be used in both anaerobic systems, in which they act as potentially recyclable oxidants, and aerobic systems, where they are used simultaneously with oxygen and act as a catalyst.[10, 11] Conventionally studied POMs include, as examples, PV_2Mo_{10}, PVW_{11}, $SiVW_{11}$,

SiV_2W_{10}, and $AlVW_{11}$ in their acid forms. These are Keggin anions with a general formula α-$[XM_{12}O_{40}]^{m-}$, where X represents the metal cation such as Al^{III}, Si^{IV} or P^{V}, and M represents the d^0 metal cations such as W^{VI}, Mo^{VI}, or V^{V}.

Ionic liquids (ILs), molten salts with melting points < 100 °C, have been used in a growing number of research applications due to their unique solvent properties and specificities that can be achieved by varying the structures of the cations and anions.[12] Certain ILs such as 1-ethyl-3-methylimidazolium acetate ([C2C1Im][OAc]), 1-butyl-3-methylimidazolium acetate ([C4C1Im][OAc]), 1-butyl-3-methylimidazolium methylsulfate ([C4C1Im][$MeSO_4$]) have been shown to dissolve cellulose, lignin, and even whole plant cell walls and have opened new opportunities in biomass deconstruction and conversion.[13-16] Recently, novel POM-ILs containing organic cations combined with Keggin anions have been reported for lignin valorization.[17, 18] There are a few examples of POM-ILs systems for delignification, producing functionalized aromatics such as vanillin and syringaldehyde.[19-21] Keggin-type POMs in either acidic form, $H_5[PV_2Mo_{10}O_{40}]$, or IL-based form, $[C2C1Im]_5[PV_2Mo_{10}O_{40}]$, can efficiently catalyze the solubilization and delignification of softwood in the IL ([C2C1Im][OAc]).[19] Pd and $[PW_{12}O_{40}]$-ILs composite supported on SiO_2 has been employed for degradation of lignin.[22] Furthermore, Keggin anions $[PW_{12}O_{40}]^{3-}$ and $[SiW_{12}O_{40}]^{3-}$ based ILs can be directly used as biomass solvents.[23] The combination of POM and ILs has improved the degree of delignification and showed more superiority with a simpler, less chemically intensive, overall process compared with the industrial Kraft process. However, the fundamental dissolution mechanism of lignin in POM-ILs systems is still lacking.

In this work, quantum chemical calculations and molecular dynamics simulations of the lignin model compound guaiagylglycerol beta-guaiacyl ether (GGE), which contains a β-O-4 bond (the most dominant bond moiety in lignin), and POM-IL ($[C4C1Im]_3[PW_{12}O_{40}]$) were performed to understand the microscopic dissolution mechanism of lignin in the POM-IL systems. The anchoring $[C4C1Im]^+$ on the POM surface has been systematically investigated. This fundamental understanding of the properties and catalytic performance of POM-IL is essential for the design and development of POM-IL systems. Furthermore, the detailed interactions, which are essentially H-bonding interactions between lignin model compound and Keggin-type

POM-IL, were studied to understand the lignin dissolution/deconstruction mechanism. The proposed work will not only provide fundamental understanding of novel POM-IL structural characteristics but will also provide fundamental models of the dissolution mechanism of lignin by POM-IL.

2. Computational method

2.1 Quantum Chemistry Calculations

All density functional theory (DFT) calculations were performed using the Gaussian 16 program.[24] Structural optimizations were carried out using the M06L functional[25] with the 6-31g** basis sets for main group elements and the pseudopotential basis sets LANL2DZ for the metal elements. Vibrational frequencies were also calculated at the same level of theory. All structures discussed in the present study were verified as minima without any negative vibrational frequency. To get more accurate energy data, single point calculations were performed at the M06L/def2-TZVP level, which provides more reliable interaction energies based on the CCSD(T) values.[26] The correction factor for the basis set super position error (BSSE) was also considered and the interaction energy (ΔE) of the conformers was defined as follows:

$$\Delta E = 627.51 * [E_{ab} - (E_a + E_b)] + \Delta E_{BSSE}, kcal/mol \quad (1)$$

Additionally, symmetry-adapted perturbation theory (SAPT)[27, 28] was applied by using Psi4[29] to decompose the interaction energies in the complexes. The interaction energy was further split into four chemically meaningful components:

$$\Delta E = \Delta E_{els} + \Delta E_{ex} + \Delta E_{ind} + \Delta E_{disp}, kcal/mol \quad (2)$$

where ΔE_{els} corresponds to the classic electrostatic interaction between the promoted fragments as they are brought to their positions in the final complexes, ΔE_{ex} is the exchange repulsion term from the Pauli repulsion effect and is invariably positive, ΔE_{ind} is the induction term, which is sometimes referred to as the orbital interaction term or the polarization term, and ΔE_{disp} is the dispersion energy, which represents the amount of energy required to promote the separated fragments from their equilibrium geometry to the structure they will take up in the combined molecule.[30] To further analyze H-bonds in the system, the electron density, potential energy density, and laplacian value at the critical points were generated by Multiwfn program.[31]

2.2 Molecular Dynamics Simulations

Molecular dynamics (MD) simulations were performed using the Gromacs 5.1.1 software package. For the simulation systems containing one lignin chain, which was obtained from Petridi *et al*.,[32] and 100 pairs of $[C4C1Im]_3[PW_{12}O_{40}]$ were randomly built using PACKMOL.[33] The force field for the imidazolium cation, lignin and $[PW_{12}O_{40}]^{3-}$ were obtained from Liu's work[34], the work reported by Petridis *et al*[32] and the parameters reported by López *et al* [35], respectively. The force field of Keggin's POMs have been widely used in previously published work, and excellent agreement has been reported between computed and experimental data for diffusion coefficients and for the most likely protonated terminal oxygens[36, 37]. Periodic boundary conditions (PBC) were used with an initial box size of 7 x 7 x 7 nm in x, y, z directions. The Particle-mesh Ewald summation[38] was taken in the calculation of long-range electrostatic interactions with a cutoff of 1.2 nm. All covalent bonds were constrained at their equilibrium values using the LINCS algorithm.[39] To remove atomic collision, the initial system was minimized by the steepest descent method until the minimum force (100 kJ $mol^{-1}nm^{-1}$). Then the geometries were equilibrated for 500 ps under NVT with a V-rescale thermostat at room temperature (298K). Another 5 ns annealing was used by increasing the temperature from 298 to 473K to simulate the system at 473K, which was based on the experiment of Abia *et al*.[23] Finally, production runs of 100 ns were carried out in the NPT ensemble with a 2 fs timestep. The last 50 ns trajectory in the production simulations was analyzed.

3. Results and discussion

3.1 Geometrical Features

The optimized structures of POM, $[C4C1Im]^+$, and guaiacyl glycerol-β-guaiacyl ether (GGE), which is the model compound representing the most abundant β-O-4 linkages in lignin, are presented in Fig. 1. It is well known that the Keggin-type $[PW_{12}O_{40}]^{3-}$ anion contains a cage of tungsten atoms linked by oxygen atoms with a tetrahedral phosphate group. The arranged 40 oxygen atoms can be divided into three types of oxygen: central oxygen atom bound to (Oc), bridging two mental atoms (Ob), and terminal oxygen atom

bound to the tungsten atom (Ot). The selected geometrical parameters of POM anion optimized at M06L/6-31g** level (LANL2DZ basis sets on metal atoms) are listed in Table S1. The maximum deviations between DFT optimized structures and the experimental data was only 0.02 Å in the W-Oc and P-Oc.[40] The same method and similar discrepancy had also been reported elsewhere.[41, 42] As shown in Fig. 1, there are two different regions: the A region connecting four terminal Ot and the B region connecting three terminal Ot. For the $[C4C1Im]^+$ cation, the imidazolium ring exhibits a planar structure. In order to give a visual understanding of the possible interaction modes among $[PW_{12}O_{40}]^{3-}$, $[C4C1Im]^+$ and GGE, the electrostatic potential surface was calculated and mapped onto the surface of the structures (bottom of Fig. 1). In the $[PW_{12}O_{40}]^{3-}$ anion, the electrostatic potential of the bridging oxygen (-0.266 a.u. for Ob) atoms are more negative than those of the terminal oxygen atoms (-0.258 a.u. for Ot), which is consistent with previous studies.[43] For the $[C4C1Im]^+$ cation, the most positive position is the H2 (0.179 a.u.). A series of conformational isomers of the GGE model compound were calculated and are listed in Fig. S1. The hydroxyl group on the γ-carbon of GGE-1 is very close to the methoxy group on benzene ring, putting the oxygen atom in position to attract hydrogen atoms to form H-bonds, which stabilizes the isomer at the lower energy. In addition, according to the previous DFT study on the dissolution of lignin in ILs[44], Zhang *et al*. also reported GGE-1 was more stable in the natural structure of lignin polymers. Furthermore, there are three kinds of oxygen atoms named α, β, and γ in the inter-chain of GGE. The electrostatic potentials of Oα, Oβ, and Oγ in GGE are also different with 0.034, 0.040 and 0.052 a.u., respectively.

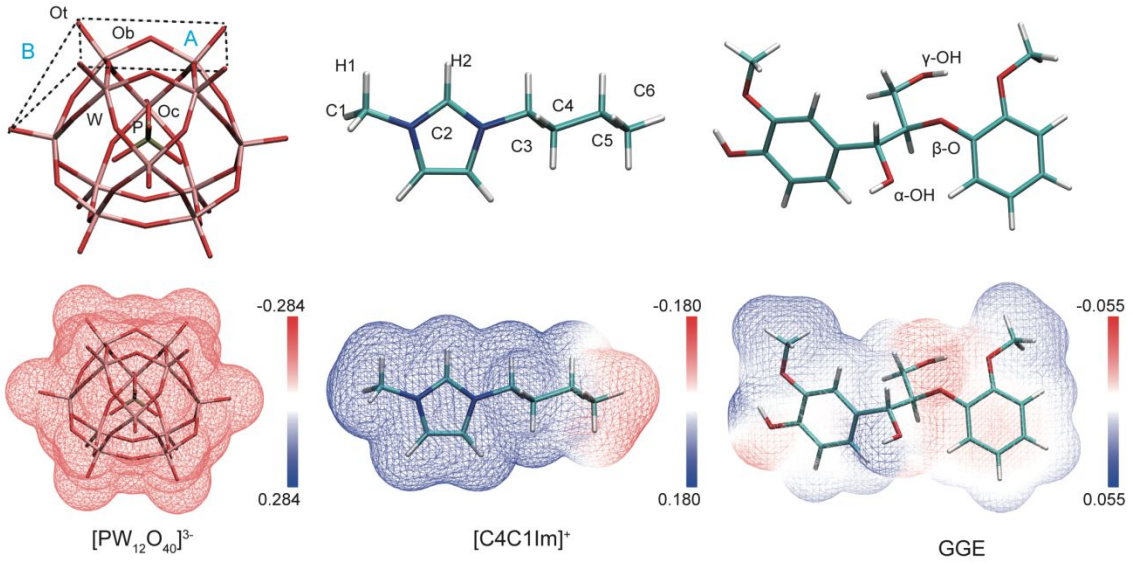

Fig. 1 The optimized geometries of the isolated $[PW_{12}O_{40}]^{3-}$ anion, $[C4C1Im]^{+}$ cation and GGE. The electrostatic potential surfaces of anion and cation are displayed at the bottom row, where the red and blue regions represent the negative and positive electrostatic potentials, respectively.

3.2 Anchor $[C4C1Im]^{+}$ on $[PW_{12}O_{40}]^{3-}$ Surface.

3.2.1 The interaction of $[C4C1Im]^{+}$ with $[PW_{12}O_{40}]^{3-}$

As a novel, organic-inorganic hybrid material, it is of great interest to investigate the POM-ILs structures.[45, 46] Starting from all possible sites of an anchor on the Keggin-type $[PW_{12}O_{40}]^{3-}$ surface for $[C4C1Im]^{+}$ studied here, we performed the geometric optimization without any restriction at M06L/6-31g** level (LANL2DZ basis sets on metal atoms). Due to the A and B regions in the $[PW_{12}O_{40}]^{3-}$ surface, the $[C4C1Im]^{+}$ can mainly anchor four different kinds geometries on the POM surface. The optimized structures and interaction energies of anchoring $[C4C1Im]^{+}$ on A, B, and A/B region in POM surface are shown in Fig. 2. As indicated by the dashed lines in Fig. 2, it is clear that the relatively most stable conformation of the complex is where the C2-H of $[C4C1Im]^{+}$ is anchored to the bridging/terminal oxygen of POM (Fig. 2, conformation A). The corresponding H-bond lengths, bond angles and interaction energies of $[C4C1Im]^{+}$ $[PW_{12}O_{40}]^{3-}$ structures are summarized in Table S2. The bond lengths of C2-H2···Ob/Ot range from 1.94 to 2.04 Å, which is the sum of van der Waals atomic radii (2.72 Å) for O···H bonds.[47] Furthermore,

the interaction energies calculated at M06L/6-31g** (LANL2DZ basis sets on metal atoms) are nearly 3-4 kcal/mol lower than those calculated at M06L/def2-TZVP. The interaction energies of anchoring $[C4C1Im]^+$ on A, B and two possible orientations in the A/B region using M06L/def2-TZVP level corrected by BSSE are -166.20, -156.95, -160.98 and -154.89 kcal/mol, respectively. Comparing the interaction energies of anchoring $[C4C1Im]^+$ at different sites, the more stable structure is formed when $[C4C1Im]^+$ anchors in the A region of $[PW_{12}O_{40}]^{3-}$ surface (Fig. 2A).

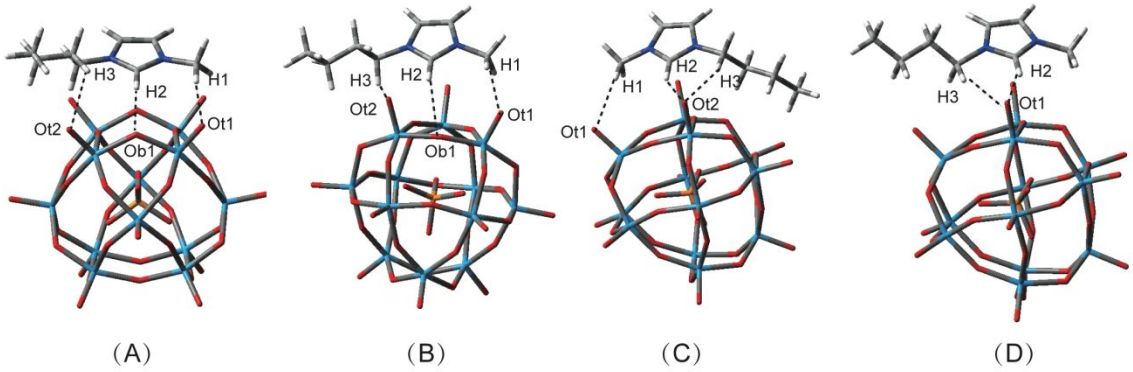

Fig. 2. Optimized conformation of four $[C4C1Im]^+$ $[PW_{12}O_{40}]^{3-}$ structures: (A) anchor $[C4C1Im]^+$ on A region (-166.20 kcal/mol), (B) anchor $[C4C1Im]^+$ on B region (-156.95 kcal/mol) (C) anchor $[C4C1Im]^+$ on A/B region (-160.98 kcal/mol) and (D) anchor $[C4C1Im]^+$ on A/B region (-154.89 kcal/mol).

The atoms in molecules theory (AIM) has been widely applied to many DFT calculations to analyse interatomic interaction,[48, 49] and we have used it here to examine the intermolecular interactions between $[PW_{12}O_{40}]^{3-}$ and $[C4C1Im]^+$. The H-bond properties, including bond energies (E_{HB}) and electron density [($\rho(r)$], of anchoring $[C4C1Im]^+$ on POM surface are listed in Table S3. As important measures of H-bond formation, the $\rho(r)$ and corresponding Laplacian value [$\nabla^2\rho(r)$] at the critical points range from 0.009 to 0.028 and 0.031 to 0.052 a.u., respectively, placing them within the standard for defining the existence of H-bonds.[50, 51] Taking, as an example, the structure in which $[C4C1Im]^+$ is anchored at the A region of the POM surface, both C-H···Ot and C-H···Ob H-bonds are formed between $[C4C1Im]^+$ and $[PW_{12}O_{40}]^{3-}$. The bond energies of C2-H2···Ob1, C1-H1···Ot1 and C3-H3···Ot2 are -23.03, -14.92 and -8.27 kcal/mol, respectively. This

indicates that C2-H2···Ob1 is stronger than the H-bonds formed with the terminal oxygen of POM. The simulation also provides theoretical support for formation of H-bonds between POM anion and the C-H of the imidazolium cation reported by the previous experimental observation.[52, 53]

3.2.2 The interaction of $[C4C1Im]_3[PW_{12}O_{40}]$ ion pairs

Ion pairs or clusters are the main structural elements existing in the structure of ILs.[54] We also investigated the geometry of $[C4C1Im]_3[PW_{12}O_{40}]$ to better understand its crystal structure. The optimized geometry and interaction energy are shown in Fig. 3 and Table S4 and show the structures are stabilized by formation of multiple H-bonds between $[C4C1Im]^+$ and $[PW_{12}O_{40}]^{3-}$ cage, forming a cationic shell was around the anion. Different geometries are formed when the $[C4C1Im]^+$ is anchored to different regions of POM. The calculated interaction energies at the M06-2X/def2-TZVP level corrected by BSSE are approximatley -360 kcal/mol, which reflects the stability of the POM surrounded by $[C4C1Im]^+$ clusters. Based on the calculations in Sec 3.2.1, $[C4C1Im]^+$ is more likely to anchor to the A region of POM, indicating that $[C4C1Im]^+$ coordinated by the four terminal oxygen atoms is the more probable conformation for $C4C1Im/PW_{12}O_{40}$. The energetically most stable (Table S4, ΔE_{2C} = -364.58 kcal/mol**)** structure of $[C4C1Im]_3[PW_{12}O_{40}]$ is shown in Fig. 3 (C), where the three $[C4C1Im]^+$ cations mainly anchor to the A region of $[PW_{12}O_{40}]^{3-}$. Natural population analysis (NPA) is one of the simplest and intuitive descriptions of the charge distribution in chemical systems,[55, 56] and results for NPA charge analysis and assignment of atomic charges of $[C4C1Im]_3[PW_{12}O_{40}]$ at the M06L/6-31g** level are shown in Table S5. These results show that the NPA charge transfer energies in $[C4C1Im]^+$ moieties are 24.47, 9.41 and 20.71 kcal/mol. This charge reorganization contributes to the activation of POM-IL. The cations in $[C4C1Im]_3[PW_{12}O_{40}]$ appears to stabilize the geometry by offering strong and positively charged sites, indicating the POM anion is a good H-bond acceptor.

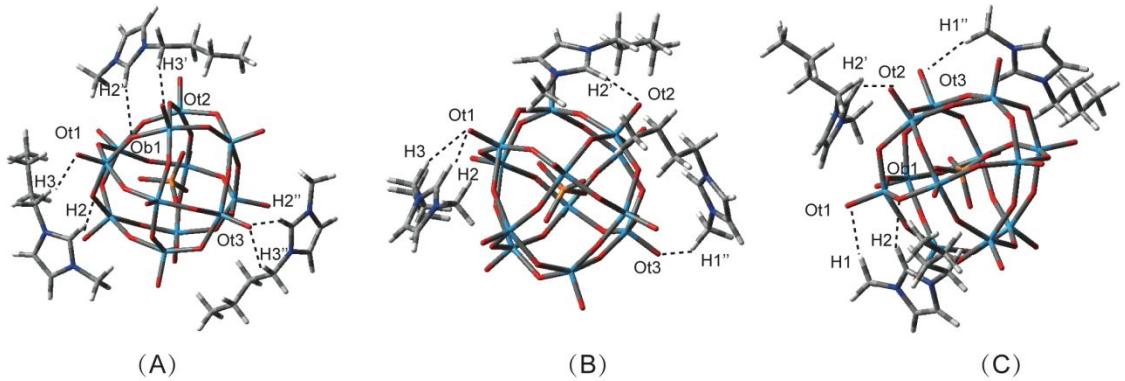

Fig. 3. Optimized three kinds of $[C4C1Im]_3[PW_{12}O_{40}]$ ion pairs where the $[C4C1Im]^+$ anchors at a different area of $[PW_{12}O_{40}]^{3-}$ surface.

3.3 The Interaction of Lignin and POM-IL

3.3.1 The Interaction of GGE-Anion, GGE-Cation, and GGE-H_2O

Solvation Model based on Density (SMD) models are quantum mechanical continuum universal solvation models that can be applied to predict the free energy of solvation of any solute in any solvent following specification of various macroscopic solvent parameters. Bernales *et al* proposed the SMD for ionic liquids (SMD-GIL) solvation model to describe the ILs solvent effects.[57] In our previous work, the reaction barrier had been compared in SMD-GIL and gas phase. The SMD-GIL solvation model provides a liquid environment and the reaction barrier in SMD is a little lower than that of vacuum state.[58] The macroscopic properties of the substance could be manifested through the joint actions of the molecules. Like the microscopic mechanism of lignin solubilization in ILs, several publications[59-61] have reported that interaction energies are relevant for solubilization analysis. To investigate the role of the anion, cation and H_2O in the dissolution of lignin, the structures of GGE-POM, GGE-C4C1Im, GGE-OAc, and GGE-H_2O were studied. Optimized conformations of the four complexes calculated from different initial starting configurations are depicted in Fig. S2 and H-bonds and interaction energies are provided in Table S6. These data show there a number of H-bonds formed in all four of the complexes, which is consistent with studies reporting that H-bonding interactions between lignin and the solvent play a vital role in dissolution of lignin .[44, 62] The interaction energies were calculated using M06-2X/def2-TZVP level and corrected by BSSE in the GGE-POM

system and are vary between -21.81 and -32.97 kcal/mol. These energies are stronger than the interaction energies between GGE and C4C1Im (-19.67 to -22.73 kcal/mol), suggesting the POM plays a stronger role in lignin dissolution. The POM anion also induces large bended conformation of GGE (Fig. S2, B, C), supporting the POM anion playing a critical role in lignin degradation and solubilization. The changes in bond length for GGE interacting with POM are shown in Table S7. The bond length of C2-Oα (original 1.41980 to 1.43615, 1.43170 and 1.43599 Å) and C3-Oβ (original 1.43844 to 1.46091, 1.45729 and 1.45019 Å) in GGE interacting with POM and corresponding to the structures in Fig. S2 (A-C) are longer than those in GGE, which likely facilitates bond cleavage and loss of the hydroxyl group (Oα-H and Oβ-H). Parthasarathi *et al.* calculated the dissociating linkages of 65 lignin model compounds also demonstrated that the C-O bond was easier dissociated than C-C bond linkages.[63]

For the GGE-C4C1Im conformers, there are three kinds of interaction sites on GGE, α-OH, γ-OH, and Oβ. The interaction energies calculated using M06-2X/def2-TZVP level and corrected by BSSE of GGE-C4C1Im when the cation interacts at α-OH, γ-OH and Oβ are -22.73, -22.46 and -19.67 kcal/mol, respectively. Comparing the interaction energies of the different sites, the order of C4C1Im to form H-bonds with GGE follows: α-OH >γ-OH >Oβ. For the GGE-OAc conformers, the interaction energies of H-bonds formed between OAc and α-OH, γ-OH are -29.96 and -24.53 kcal/mol, respectively. It can be concluded that when H-bonds formed between the electronegative area (oxygen) of OAc and the α-OH of GGE, the interaction energy appears stronger. The stronger interaction energies between GGE and anions, indidcates that anions play a critical role in the dissolution/degradation of lignin. The interaction energy of GGE with H_2O, calculated at the M06L/df2-TZVP level, ranges between -5.76 and -6.54 kcal/mol, which is consistent with lignin not being soluble in water due to the weak interaction energy of GGE-H_2O conformers.

Energy decomposition analysis is a valuable tool for investigating the physical contributions of the various energetic components contributing to the total interaction energy.[64] The energy decomposition analyses for GGE-POM, GGE-C4C1Im, GGE-OAc, and GGE-H_2O are presented in Table S8. In GGE-POM, the electrostatic attraction, exchange repulsion, induction and dispersion energies account for 27.5%, 34.2%, 10.7%,

298 and 27.6%, respectively. This result confirms that the POM-ILs have a strong
299 Coulombic interactions due to the high melting temperature of the crystalline lattice.[65] For
300 the GGE-anion interactions, like GGE-POM and GGE-OAc, the electrostatic attraction
301 energy is about 5 to 17 kcal/mol stronger than that of GGE-C4C1Im, which indicates
302 anions play a critical role in the lignin dissolution. In the GGE-POM and GGE-C4C1Im
303 structures, the dispersion energies are more obvious than those of GGE-OAc and GGE-
304 H_2O. It further illustrates that using the dispersion-correlation M06L functional gives more
305 desirable calculations.[66, 67]

306 Independent Gradient Model (IGM) analysis has been employed as one of the most
307 useful tools to study the noncovalent interaction.[68] To investigate the types of interactions
308 between GGE and isolated C4C1Im/POM, IGM analysis was performed using the most
309 stable structures of GGE-POM and GGE-C4C1Im. The interaction isosurfaces were
310 plotted and are shown in Fig. 4. For GGE-POM, a large conformational bend in GGE was
311 induced by the POM anion, and H-bonds were formed between GGE and both sides of the
312 POM. For GGE-C4C1Im, strong H-bonds were observed between the C2-H of $[C4C1Im]^+$
313 and the α-OH of GGE (a strong H-bond is highlighted by the red circle in Fig. 4). As
314 reported by Janesko,[69] stronger interactions with lignin resulted in the extended π-system
315 of imidazolium ILs. Also, the other large green surface in the isosurface represents strong
316 π-π stacking effects between the two rings.
317

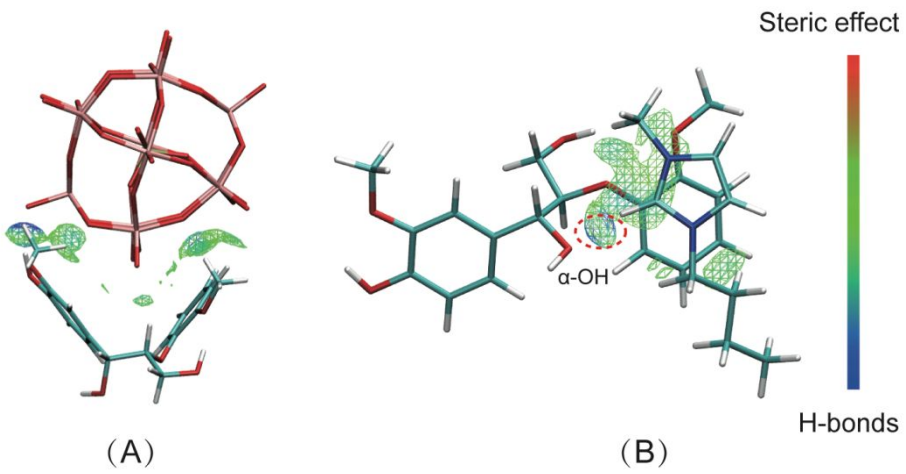

Fig. 4 Isosurfaces (isovalue =0.5 a.u.) of (A) GGE-POM and (B) GGE-C4C1Im. Blue indicates strong attractive interaction like H-bonds, green indicates π-π interactions and red indicates steric hindrance.

3.3.2 The interaction of GGE and [C4C1Im]$_3$[PW$_{12}$O$_{40}$] ion pair

Six starting conformations of GGE-[C4C1Im][$PW_{12}O_{40}$] and GGE-[C4C1Im]$_3$[$PW_{12}O_{40}$] structures were optimized to obtain the possible interaction modes between GGE and POM-IL (Fig. 5). The corresponding interaction energies and the bond changes are listed in Table S9 and Table S10, respectively. In Fig.5, the cations mainly interact with POM to form cationic shells and POM mainly interacts with lignin which further verified that POM played a critical role in the dissolution of lignin. The changes of C-O bond length (Table S10) were not obvious when there are more cations molecular, because the cations mainly interact with POM to form a shell cage. The BBSE corrected interaction energies at the M06L/def2-TZVP level for different GGE-[C4C1Im]$_3$[$PW_{12}O_{40}$] structures were all approximately -387 kcal/mol. The relative energies of different modes are inapparent due to the large system. To compare with the interaction of POM-IL, the interactions between GGE and [C4C1Im][OAc] were calculated and are shown in Fig. S3 and listed in Table S11. The interaction energies of A, B, C are -121.25, -127.25 and -128.70 kcal/mol, respectively. The interaction of GGE-[C4C1Im][OAc] is more intensive at α-OH than at γ-OH. Furthermore, to investigate the interaction in the GGE-ILs system, IGM analysis of GGE-[C4C1Im][OAc] and GGE-[C4C1Im]$_3$[$PW_{12}O_{40}$] were performed and results are shown in Fig. S4. For GGE-[C4C1Im][OAc], strong H-bonds were formed

between OAc and α-OH of GGE. Between the benzene ring and imidazolium ring, there is another large area (green) corresponding to π-π interaction. For GGE-$[C4C1Im]_3[PW_{12}O_{40}]$, $[C4C1Im]^+$ forms multiple H-bonds around POM due to the large molecule of the anion. The interaction of GGE and POM-IL is mainly through interactions with the anion, while cationic shells around the POM form the main interactions of POM-IL with lignin. Taken together, these results show that the POM plays an important role in the dissolution of lignin.

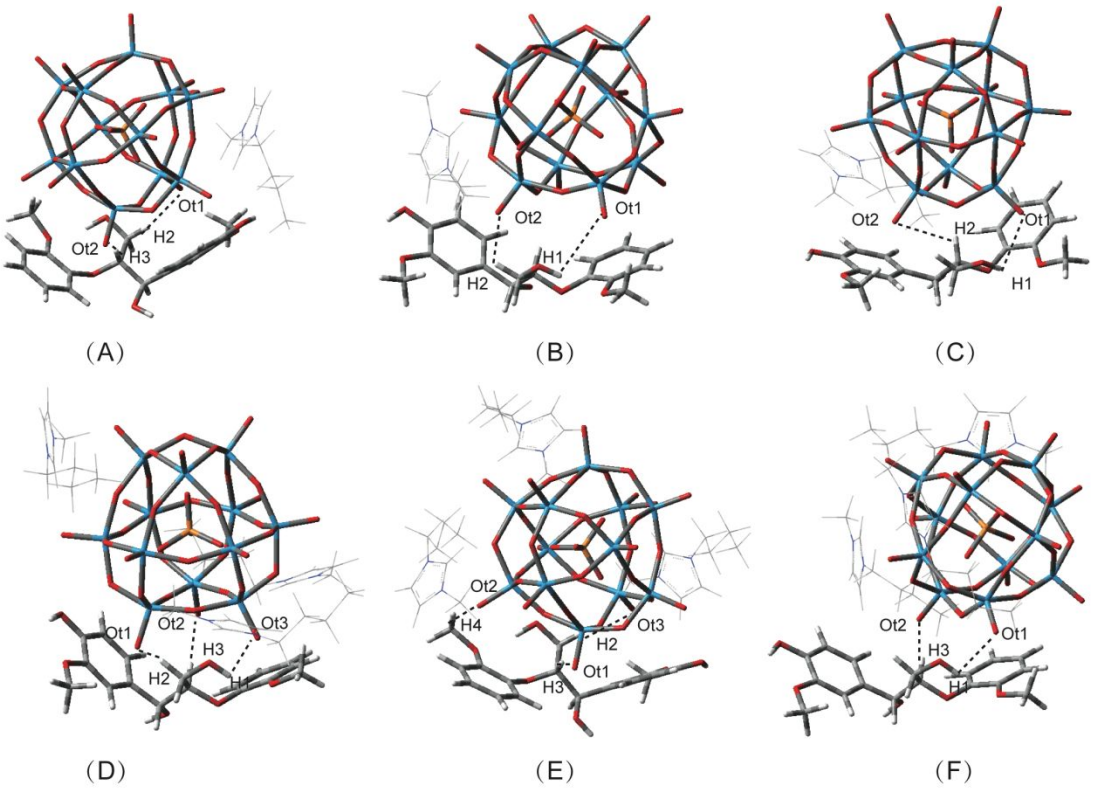

Fig. 5 Optimized conformations of GGE-$[C4C1Im][PW_{12}O_{40}]$ (A-C) and GGE-$[C4C1Im]_3[PW_{12}O_{40}]$ (D-F) complexes.

To gain additional insights into the solubilization of lignin in POM-IL, molecular dynamics (MD) simulations were performed on systems of lignin and POM-IL. The interaction energies of lignin with C4C1Im and POM are listed in Table 1. It was found that the total interaction energy of Lignin-POM (-716.92 kcal/mol) is much stronger than that of Lignin-C4C1Im (-495.65 kcal/mol), providing additional evidence that lignin interactions with POM play a critical role in dissolution of lignin. The interaction energy

between lignin and C4C1Im mainly comes from the Lennard-Jones (LJ) potential, while the interaction energy between lignin and POM mainly comes from coulombic interaction. To characterize the structural features of the bulk lignin plus POM-IL system radial distribution functions g(r) were calculated from the MD simulations using equation 3:

$$g_{ij}(r) = \frac{N_{ij}(r, r + \Delta\ r)V}{4\pi r^2\ \Delta\ r N_i N_j} \qquad (3)$$

where r represents the distance between i and j atoms, N_i and N_j represent the numbers of i and j atoms, $N_{ij}(r, r+\Delta r)$ represents the number of j atoms around i within a shell from r to $r+\Delta r$, and V is the volume of system. The g(r) for the center of mass of Lignin-C4C1Im and Lignin-POM, as well as atom-atom distributions of Ob (POM)-Oβ (lignin) and Ot (POM)-Oβ (lignin), are shown in Fig. 6. As shown in Fig. 6 (A-B), the peak at ~1.3Å suggests there is more concentrated distribution of POM anion than $C4C1Im^+$, occupying the secondary solvation shell. However, the POM anion is farther from lignin than the cation because of the larger size of POM. In Fig. 6 (C-D), pronounced peaks located ~0.35 Å for Ot (POM)-Oβ (lignin) indicates that Ot of POM is closer to Oβ (lignin) than that of Ob. And the coordination numbers of Ot (POM)-Oβ (lignin) are larger than that of Ob (POM)-Oβ (lignin). Furthermore, the peak height of Ot (POM)-Oβ (lignin) is higher than that of Ob (POM)-Oβ (lignin), revealing that the oxygen in the bridge of POM has a weaker interaction with Oβ than that of the POM's terminal oxygen.

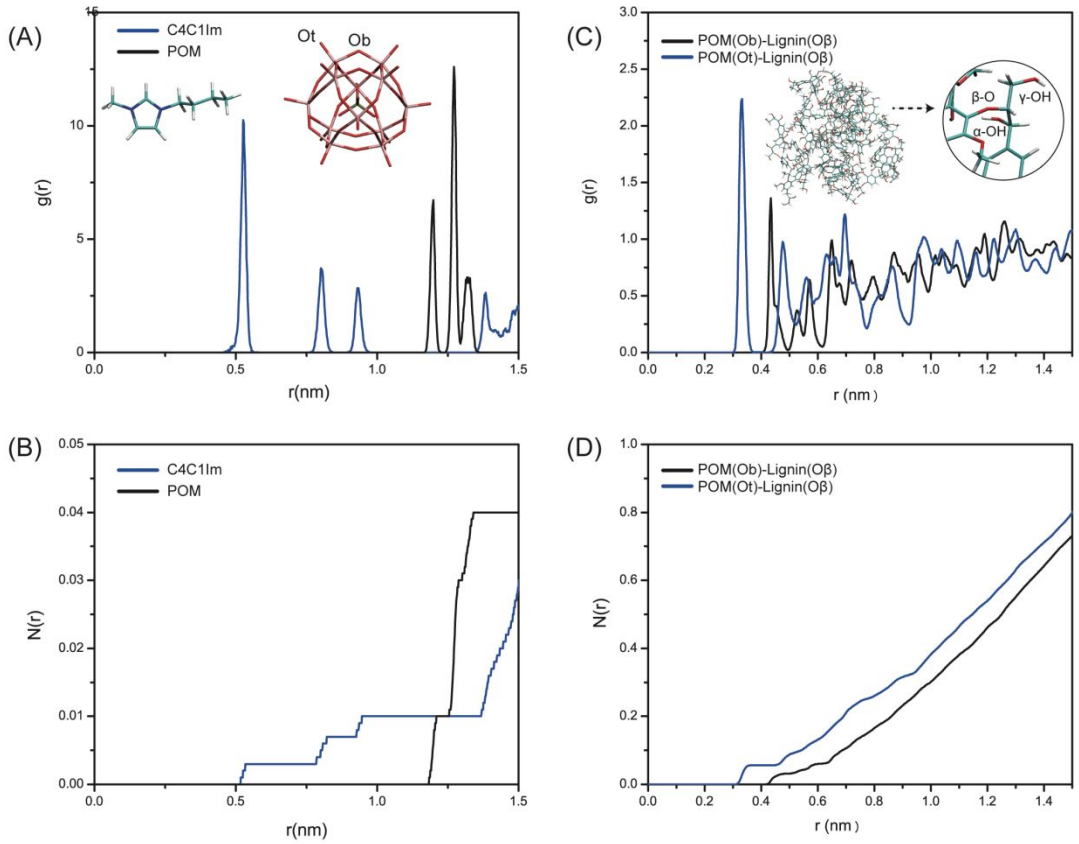

Fig. 6 (A) Radial distribution functions for the center mass of Lignin-C4C1Im and Lignin-POM (B) corresponding coordination numbers (C) Radial distribution functions for Ot, Ob of POM around Oβ of lignin and (D) corresponding coordination numbers.

Table 1 Interaction energies (in kcal/mol) of lignin and $[C4C1Im]_3[PW_{12}O_{40}]$ based on MD simulations.

	E_{coul}	$E_{L\text{-}J}$	E_{total}
$[C4C1Im]^+$	-150.75	-344.90	-495.65
$[PW_{12}O_{40}]^{3-}$	-445.07	-271.85	-716.92

4. Conclusion

As novel green catalyst and solvent systems, POM-ILs have shown great promise for delignification of biomass. However, the microscopic mechanism, which provides insights for further engineering of improved biomass pretreatment approaches, for lignin

dissolution remains unknown. In this work, we used a model lignin compound containing a β-O-4 linkage, which is the most abundant linkage in the lignin structure, to investigate the interactions between lignin and POM-IL that provide the molecular driving forces for dissolution of lignin. First, the interactions of POM-IL composed of $[PW_{12}O_{40}]^{3-}$ and $[C4C1Im]^{+}$ were studied using DFT calculations. Based on the computed interaction energies, more stable structures are formed when $[C4C1Im]^{+}$ anchors in the connecting four terminal oxygen containing region of the $[PW_{12}O_{40}]^{3-}$ surface. The cations in POM-IL stabilize this geometry by offering strong and positively charged sites and the POM anion is a strong H-bond acceptor. Second, to investigate the dissolution mechanism of lignin in POM-IL, the interactions of GGE with the anion and cation of POM-ILs and with H_2O were studied by DFT calculations. The interactions of GGE with the POM-IL anion were calculated to be much stronger than the interactions between GGE and POM-IL cation, suggesting the anion of POM plays a critical role in lignin dissolution. The interactions of the POM-IL anion forced GGE into a highly bent conformation, further suggesting a mechanism by which the lignin backbone is exposed to the solvent and made it easier to degrade. Based on our calculations H-bonds formed between lignin and the POM-IL anion together with π-π interaction formed between the POM-IL cation and lignin are the main interactions and driving forces for dissolution of lignin. Third, to obtain additional insights into the solubilization of lignin, MD simulations were performed on systems of GGE and POM-IL. Results from these simulation further confirmed that lignin interactions with the POM-IL anion play a critical role in dissolution of lignin. The data from quantum calculations and MD simulations presented here provide fundamental insights into the mechanisms by with POM-ILs interact with lignin and drive lignin dissolution and models of the how novel POM-ILs structural characteristics might be designed to improve dissolution of lignin.

Author Information

Corresponding Author

Corresponding author, E-mail: klsale@lbl.gov, nsun@lbl.gov

Associated Content

Supporting Information

The selected bond distance of POM, H-bonds, interaction energies and AIM analysis of $[C4C1Im]^+$ $[PW_{12}O_{40}]^{3-}$ complex of the POM-ILs; interaction energies, NPA analysis of $[C4C1Im]_3[PW_{12}O_{40}]$; energy decomposition; IGM analysis for GGE-POMILs and GGE-ILs.

Conflicts of interest

There are no conflicts of interest to declare.

Acknowledgment

This research was financially supported by the National Key R & D Program of China (2017YFB0307303) and financial support from the program of China Scholarships Council (201806350089). The authors from the ABPDU acknowledge the support from the US Department of Energy's Bioenergy Technologies Office (BETO) which is part of the Office of Energy Efficiency and Renewable Energy (EERE).

References:

1. S. Kim, S. C. Chmely, M. R. Nimlos, Y. J. Bomble, T. D. Foust, R. S. Paton and G. T. Beckham, *The Journal of Physical Chemistry Letters*, 2011, **2**, 2846-2852.
2. J. Zakzeski, P. C. Bruijnincx, A. L. Jongerius and B. M. Weckhuysen, *Chemical Reviews*, 2010, **110**, 3552-3599.
3. J. M. Nichols, L. M. Bishop, R. G. Bergman and J. A. Ellman, *Journal of the American Chemical Society*, 2010, **132**, 12554-12555.
4. F. H. Isikgor and C. R. Becer, *Polymer Chemistry*, 2015, **6**, 4497-4559.
5. F. P. Bouxin, A. McVeigh, F. Tran, N. J. Westwood, M. C. Jarvis and S. D. Jackson, *Green Chemistry*, 2015, **17**, 1235-1242.

6. L. Chen, J. Xin, L. Ni, H. Dong, D. Yan, X. Lu and S. Zhang, *Green Chemistry*, 2016, **18**, 2341-2352.
7. N. A. DeLucia, N. Das, S. Overa, A. Paul and A. K. Vannucci, *Catalysis Today*, 2018, **302**, 146-150.
8. Y. Chen, X. Cao, S. Zhu, F. Tian, Y. Xu, C. Zhu and L. Dong, *Bioresource technology*, 2019.
9. B. Bujanovic, S. Ralph, R. Reiner, K. Hirth and R. Atalla, *Materials*, 2010, **3**, 1888-1903.
10. T. Voitl, M. V. Nagel and P. R. Von Rohr, *Holzforschung*, 2010, **64**, 13-19.
11. I. B. Baguc, S. Saglam, I. E. Ertas, M. N. Keles, M. Celebi, M. Kaya and M. Zahmakiran, *ChemistrySelect*, 2017, **2**, 2487-2494.
12. J. Dupont, R. F. de Souza and P. A. Z. Suarez, *Chemical Reviews*, 2002, **102**, 3667-3692.
13. Y. Pu, N. Jiang and A. J. Ragauskas, *Journal of Wood Chemistry and Technology*, 2007, **27**, 23-33.
14. N. Sun, H. Rodríguez, M. Rahman and R. D. Rogers, *Chemical Communications*, 2011, **47**, 1405-1421.
15. N. Sun, R. Parthasarathi, A. M. Socha, J. Shi, S. Zhang, V. Stavila, K. L. Sale, B. A. Simmons and S. Singh, *Green Chemistry*, 2014, **16**, 2546-2557.
16. N. Sun, M. Rahman, Y. Qin, M. L. Maxim, H. Rodríguez and R. D. Rogers, *Green Chemistry*, 2009, **11**, 646-655.
17. T. Rajkumar and G. R. Rao, *Materials Letters*, 2008, **62**, 4134-4136.
18. T. Rajkumar and G. R. Rao, *Journal of Chemical Sciences*, 2008, **120**, 587-594.
19. N. Sun, X. Jiang, M. L. Maxim, A. Metlen and R. D. Rogers, *ChemSusChem*, 2011, **4**, 65-73.
20. F. Cheng, H. Wang and R. D. Rogers, *ACS Sustainable Chemistry & Engineering*, 2014, **2**, 2859-2865.
21. G. F. De Gregorio, R. Prado, C. Vriamont, X. Erdocia, J. Labidi, J. P. Hallett and T. Welton, *ACS Sustainable Chemistry & Engineering*, 2016, **4**, 6031-6036.
22. Z. Zhang, M. Liu, J. Song, H. Liu, Z. Xie, S. Liu, Q. Meng, P. Zhang and B. Han, *Green Chemistry*, 2018, **20**, 4865-4869.
23. J. A. Abia and R. Ozer, *BioResources*, 2013, **8**, 2924-2933.
24. M. J. Frisch, G. W. Trucks, H. B. Schlegel, G. E. Scuseria, M. A. Robb, J. R. Cheeseman, G. Scalmani, V. Barone, G. A. Petersson, H. Nakatsuji, X. Li, M. Caricato, A. V. Marenich, J. Bloino, B. G. Janesko, R. Gomperts, B. Mennucci, H. P. Hratchian, J. V. Ortiz, A. F. Izmaylov, J. L. Sonnenberg, Williams, F. Ding, F. Lipparini, F. Egidi, J. Goings, B. Peng, A. Petrone, T. Henderson, D. Ranasinghe, V. G. Zakrzewski, J. Gao, N. Rega, G. Zheng, W. Liang, M. Hada, M. Ehara, K. Toyota, R. Fukuda, J. Hasegawa, M. Ishida, T. Nakajima, Y. Honda, O. Kitao, H. Nakai, T. Vreven, K. Throssell, J. A. Montgomery Jr., J. E. Peralta, F. Ogliaro, M. J. Bearpark, J. J. Heyd, E. N. Brothers, K. N. Kudin, V. N. Staroverov, T. A. Keith, R. Kobayashi, J. Normand, K. Raghavachari, A. P. Rendell, J. C. Burant, S. S. Iyengar, J. Tomasi, M. Cossi, J. M. Millam, M. Klene, C. Adamo, R. Cammi, J. W. Ochterski, R. L. Martin, K. Morokuma, O. Farkas, J. B. Foresman and D. J. Fox, *Journal*, 2016.
25. Y. Zhao and D. G. Truhlar, *The Journal of chemical physics*, 2006, **125**, 194101.

26. F. Weigend and R. Ahlrichs, *Physical Chemistry Chemical Physics*, 2005, **7**, 3297-3305.
27. B. Jeziorski, R. Moszynski and K. Szalewicz, *Chemical Reviews*, 1994, **94**, 1887-1930.
28. T. M. Parker, L. A. Burns, R. M. Parrish, A. G. Ryno and C. D. Sherrill, *The Journal of chemical physics*, 2014, **140**, 094106.
29. J. M. Turney, A. C. Simmonett, R. M. Parrish, E. G. Hohenstein, F. A. Evangelista, J. T. Fermann, B. J. Mintz, L. A. Burns, J. J. Wilke and M. L. Abrams, *Wiley Interdisciplinary Reviews: Computational Molecular Science*, 2012, **2**, 556-565.
30. R. Kurczab, M. P. Mitoraj, A. Michalak and T. Ziegler, *The Journal of Physical Chemistry A*, 2010, **114**, 8581-8590.
31. T. Lu and F. Chen, *Journal of Computational Chemistry*, 2012, **33**, 580-592.
32. L. Petridis and J. C. Smith, *Journal of computational chemistry*, 2009, **30**, 457-467.
33. J. M. Martínez and L. Martínez, *Journal of computational chemistry*, 2003, **24**, 819-825.
34. Z. Liu, S. Huang and W. Wang, *The Journal of Physical Chemistry B*, 2004, **108**, 12978-12989.
35. X. Lopez, C. Nieto-Draghi, C. Bo, J. B. Avalos and J. M. Poblet, *The Journal of Physical Chemistry A*, 2005, **109**, 1216-1222.
36. T. J. Paul, T. N. Parac-Vogt, D. Quiñonero and R. Prabhakar, *The Journal of Physical Chemistry B*, 2018, **122**, 7219-7232.
37. J. M. Gómez-Gil, E. Laborda, J. Gonzalez, A. Molina and R. G. Compton, *The Journal of Physical Chemistry C*, 2017, **121**, 26751-26763.
38. T. Darden, D. York and L. Pedersen, *The Journal of chemical physics*, 1993, **98**, 10089-10092.
39. B. Hess, H. Bekker, H. J. Berendsen and J. G. Fraaije, *Journal of computational chemistry*, 1997, **18**, 1463-1472.
40. A. J. Bridgeman and G. Cavigliasso, *The Journal of Physical Chemistry A*, 2003, **107**, 6613-6621.
41. C.-G. Liu, S. Liu and T. Zheng, *Inorganic Chemistry*, 2015, **54**, 7929-7935.
42. C.-G. Liu, M.-X. Jiang and Z.-M. Su, *Inorganic Chemistry*, 2017, **56**, 10496-10504.
43. Y. Zheng, J. Liu, X. Yang and J. Wang, *Journal of Molecular Modeling*, 2014, **20**, 2495.
44. Y. Zhang, H. He, K. Dong, M. Fan and S. Zhang, *RSC Adv.*, 2017, **7**, 12670-12681.
45. A. Misra, I. Franco Castillo, D. P. Müller, C. Gonzalez, S. Eyssautier‐Chuine, A. Ziegler, J. M. de la Fuente, S. G. Mitchell and C. Streb, *Angewandte Chemie International Edition*, 2018, **57**, 14926-14931.
46. P. G. Rickert, M. R. Antonio, M. A. Firestone, K.-A. Kubatko, T. Szreder, J. F. Wishart and M. L. Dietz, *The Journal of Physical Chemistry B*, 2007, **111**, 4685-4692.
47. A. Bondi, *The Journal of Physical Chemistry*, 1964, **68**, 441-451.
48. G. Saleh, C. Gatti and L. Lo Presti, *Computational and Theoretical Chemistry*, 2012, **998**, 148-163.
49. R. Lü, J. Lin and Z. Qu, *Computational and Theoretical Chemistry*, 2012, **1002**, 49-58.
50. P. Lipkowski, S. J. Grabowski, T. L. Robinson and J. Leszczynski, *J. Phys. Chem. A*, 2004, **108**, 10865-10872.

51. I. Rozas, I. Alkorta and J. Elguero, *Journal of the American Chemical Society*, 2000, **122**, 11154-11161.
52. W. Guan, L. Yan, Z. Su, S. Liu, M. Zhang and X. Wang, *Inorganic Chemistry*, 2005, **44**, 100-107.
53. P. Zhao, M. Zhang, Y. Wu and J. Wang, *Industrial & Engineering Chemistry Research*, 2012, **51**, 6641-6647.
54. K. Dong, L. Zhao, Q. Wang, Y. Song and S. Zhang, *Physical Chemistry Chemical Physics*, 2013, **15**, 6034-6040.
55. T. Lu and F.-W. Chen, *Acta Physico-Chimica Sinica*, 2012, **28**, 1-18.
56. R. Fu, T. Lu and F.-W. Chen, *Acta Physico-Chimica Sinica*, 2014, **30**, 628-639.
57. V. S. Bernales, A. V. Marenich, R. Contreras, C. J. Cramer and D. G. Truhlar, *J Phys Chem B*, 2012, **116**, 9122-9129.
58. Z. Ju, X. Yao, X. Liu, L. Ni, J. Xin and W. Xiao, *Industrial & Engineering Chemistry Research*, 2019, **58**, 11111-11120.
59. Y. Li, X. Liu, Y. Zhang, K. Jiang, J. Wang and S. Zhang, *ACS Sustainable Chemistry & Engineering*, 2017, **5**, 3417-3428.
60. Y. Li, X. Liu, S. Zhang, Y. Yao, X. Yao, J. Xu and X. Lu, *Phys Chem Chem Phys*, 2015, **17**, 17894-17905.
61. R. Parthasarathi, K. Balamurugan, J. Shi, V. Subramanian, B. A. Simmons and S. Singh, *J Phys Chem B*, 2015, **119**, 14339-14349.
62. Y. Zhang, H. He, Y. Liu, Y. Wang, F. Huo, M. Fan, H. Adidharma, X. Li and S. Zhang, *Green Chemistry*, 2019, **21**, 9-35.
63. R. Parthasarathi, R. A. Romero, A. Redondo and S. Gnanakaran, *The Journal of Physical Chemistry Letters*, 2011, **2**, 2660-2666.
64. M. Parafiniuk and M. P. Mitoraj, *Organometallics*, 2013, **32**, 4103-4113.
65. S. Herrmann, A. Seliverstov and C. Streb, *Journal of Molecular and Engineering Materials*, 2014, **2**, 1440001.
66. S. Luo, Y. Zhao and D. G. Truhlar, *The journal of physical chemistry letters*, 2012, **3**, 2975-2979.
67. Y. Wang, X. Jin, S. Y. Haoyu, D. G. Truhlar and X. He, *Proceedings of the National Academy of Sciences*, 2017, **114**, 8487-8492.
68. C. Lefebvre, G. Rubez, H. Khartabil, J.-C. Boisson, J. Contreras-García and E. Hénon, *Physical Chemistry Chemical Physics*, 2017, **19**, 17928-17936.
69. B. G. Janesko, *Physical Chemistry Chemical Physics*, 2011, **13**, 11393-11401.

Table of Contents

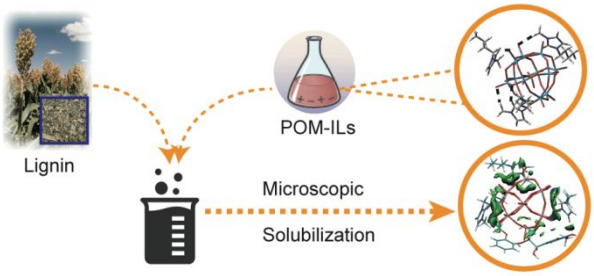

The microscopic mechanism of lignin solubilization in Keggin-type polyoxometalate ionic liquids had been studied by theoretical calculations.